Technical Notes

Experimental Study of Longitudinal Stage Separation of Two-Body Configuration in Shock Tunnel

Yue Wang,* Yunpeng Wang,† and Zonglin Jiang‡
Chinese Academy of Sciences, 100190 Beijing, People's Republic of China

https://doi.org/10.2514/1.J062135

Nomenclature

A	=	axial force, N
AoA	=	angle of attack, deg
C_A	=	axial force coefficient
C_M	=	pitching moment coefficient
C_N	=	normal force coefficient
C_p	=	pressure coefficient
D_c	=	diameter of the piston, mm
I_{zz}	=	moment of inertia about the Z axis, kg · m^2
l	=	length, mm
l_c	=	action stroke of the piston, mm
M	=	pitching moment, N · m
Ma	=	Mach number
m	=	mass, kg
N	=	normal force, N
p	=	pressure, Pa
q	=	dynamic pressure, Pa
Re	=	Reynolds number
T	=	temperature, K
t	=	time, ms
u	=	velocity in the X direction, m · s^{-1}
v	=	velocity in the Y direction, m · s^{-1}
w	=	span, mm
x	=	coordinate in the X direction
θ	=	pitching angle, deg
ω	=	pitching angle rate, deg ·s^{-1}

Subscripts

0	=	chamber condition
∞	=	freestream condition

I. Introduction

THE dynamic separation of multibody at supersonic and hypersonic speeds is complex and challenging [1–3]. The stage separation of parallel-staged two-stage-to-orbit (TSTO) vehicles has received significant attention [4,5]. The TSTO stage separation usually occurs in the hypersonic flow regime. Shock–shock and shock–boundary-layer interaction (SSI and SBLI) can be introduced into the proximity of stages but result in severe aerodynamic/aerothermodynamic loads on vehicles [6] and a high risk of separation failure, e.g., stage recontact [7]. Hence, a safe and feasible separation scheme with weak interference is expected in the TSTO mission.

Most studies concern the analysis of transverse stage separation (TSS) for parallel-staged TSTO. The orbiter is released and separated toward the normal direction of the booster, with a considerable gap between stages. Bordelon et al. [8] performed a wind tunnel test for the NASA Langley Glide-Back Booster (LGBB) TSTO model and found that the vehicle was statically unstable due to a strong bow SSI at several positions. Ozawa et al. [9] conducted wind tunnel tests on the aerodynamic interference of a simple TSTO configuration model with various gap widths at Mach 8.1. The results showed that the gap between stages affected the flow pattern, heat flux, and pressure on the wall. Due to the complexity of the dynamic test for TSTO stage separation, most studies on dynamic separation were performed by numerical methods [10]. For instance, Wang et al. [11] simulated the dynamic process of TSS of simple TSTO configuration at different incidence angles. The results demonstrated that the strong aerodynamic interference was a function of the incidence angle and gap between stages during separation.

Those studies have indicated that the TSS of parallel-staged TSTO is very sensitive to any interference in the flowfield. However, the longitudinal stage separation (LSS) for parallel-staged TSTO has not been investigated. The separation of the orbiter along the upper wall of the booster, with tiny or even no gaps, may result in a weak aerodynamic interference. Moreover, most wind tunnel tests on the stage separation of TSTO are static [12] or the "dynamic" test by a captive trajectory system [13,14] in a routine hypersonic wind tunnel (RHWT), which is a quasi-steady test method. Additionally, RHWT with a low total temperature characteristic cannot duplicate high-temperature real gas effects in a real hypersonic staging atmosphere for TSTO tests. This paper reports experimental dynamic tests of LSS for a TSTO model at Mach 7 in the JF-12 hypersonic flight duplicated shock tunnel in the Institute of Mechanics. The dynamic LSS test technique and method are detailed. Special emphasis is given to the experimental demonstration of the safety and feasibility of LSS for TSTO, detailed flow structures, wall pressure distribution, and separation motion.

II. Experimental Program

A. JF-12 Shock Tunnel and Experimental Measurements

The experiments were conducted in the JF-12 hypersonic flight duplicated shock tunnel in the Institute of Mechanics [15,16]. Pure airflow was reproduced at Mach 5–9 with a long test duration of over 100 ms (T_e). We employed a nozzle with a diameter of 2.5 m, which could generate a nominal Mach 7 hypersonic airflow. Table 1 summarizes the detailed static test of the booster and TSTO as well as LSS dynamic test conditions.

Figure 1a presents a schematic of the visualization system setup, consisting of the schlieren camera I with a frame rate of 3600 fps and the high-speed camera II with 1000 fps. Several Light Emitting Diode (LEDs) were equipped on the orbiter and orientated vertically to the observation window to be identified clearly by the image trajectory recognition method. Then the motion of the orbiter could be acquired. The pressure on the centerline of the booster wall was measured by a

Table 1   Test conditions

Test	AoA, deg	P_0, MPa	T_0, K	Ma_∞	Re_∞, m^{-1}	p_∞, Pa	q_∞, Pa
Booster	5.0	2.50	2364	6.95	8.47×10^5	447	15,134
TSTO	8.1	2.46	2378	6.93	8.33×10^5	448	15,081
LSS	8.3	2.63	2393	6.99	8.57×10^5	451	15,444
LSS	4.5	2.53	2371	6.95	8.55×10^5	454	15,351

pressure transducer with a range of 50 kPa and an accuracy of 2.5‰ F.S (Full Scale). The forces and moment of static tests were measured by a six-component strain-gage balance installed in the booster model, forming an integral structure with the sting-model support system, as shown in Fig. 1b. In addition, the balance calibration center also the moment reference point is located at $(738, -50, 0)$ mm. The capacities of the balance to the axial force, normal force, and the pitching moment are 1000 N, 2000 N, and 200 N·m, respectively.

B.   Test Model and LSS Description

In the parallel-staged TSTO model, a waverider and spaceplane serve as the booster and orbiter, respectively. Figures 2 and 3 show the photography and detail geometry of the tested TSTO model, respectively. The TSTO model is mainly made of aluminum alloy. The mass of the orbiter is about $m = 1.26$ kg. The moment of inertia in the Z axis assessed by Computer Aided Engineering (CAE) software is $I_{zz} = 1.26 \times 10^{-2}$ kg · m^2.

In the LSS test, the booster is fixed on the sting while the orbiter is thrust by the pneumatic ejection device (PED) and then separated along the upper surface of the booster. The entire separation motion of the orbiter can be divided into three phases: I) from the initial position A to the position B, where the nose of the two stages coincide; II) from the position B to the position C, where the tail of the orbiter and the nose of the booster coincides; and III) orbiter separates from the booster and flights freely. The descriptions of those positions are illustrated in Fig. 4 for clarity. The instant of LSS can be appointed based on the zero instant when the nose of the two stages coincide, i.e., position B. Thus, the instant before position B is labeled as $t < 0$ and after position B as $t > 0$.

C.   High-Speed PED

Ideally, the entire separation motion or the most significant phase II can be investigated during the test. Therefore, the high-speed motion of the orbiter requires a special PED, which can provide sufficient momentum at the initial moment of the test. As shown in Fig. 3, the pneumatic actuator includes an impact bar, a cylinder, and a high-pressure N_2 gas working medium. In the dynamic test, the high-pressure N_2 gas with high energy drives the piston to do work, and the impact bar integrates with the piston rod to apply high impulse on the orbiter and separate from the booster during the test as fast as possible.

Figure 5 presents the detailed schematic of the high-speed PED applied in the JF-12 shock tunnel. The PED consists of a high-pressure N_2 gas source, solenoid valve, pneumatic actuator, signal controller, air pump, and trigger. In the wind tunnel test, the nitrogen source is providing a high pressure of about 9 MPa N_2 gas upstream of the solenoid. When the signal controller is sending the electrical signal to the solenoid valve, the high-pressure N_2 gas passes through the solenoid valve then drives the piston to do work and to apply high impulse on the orbiter for separation by a pneumatic actuator. The signal controller and test data acquisition system as well as the operation of the shock tunnel were triggered by a synchronizer. The remained gas between the solenoid and cylinder must be sucked out by the air pump to keep the vacuum environment, or the remained gas will push the piston rod forward before the test since the vacuum of the test section causes the abort of the experiment. Because the effective test time is short and precious, the delay time and separation duration are significant.
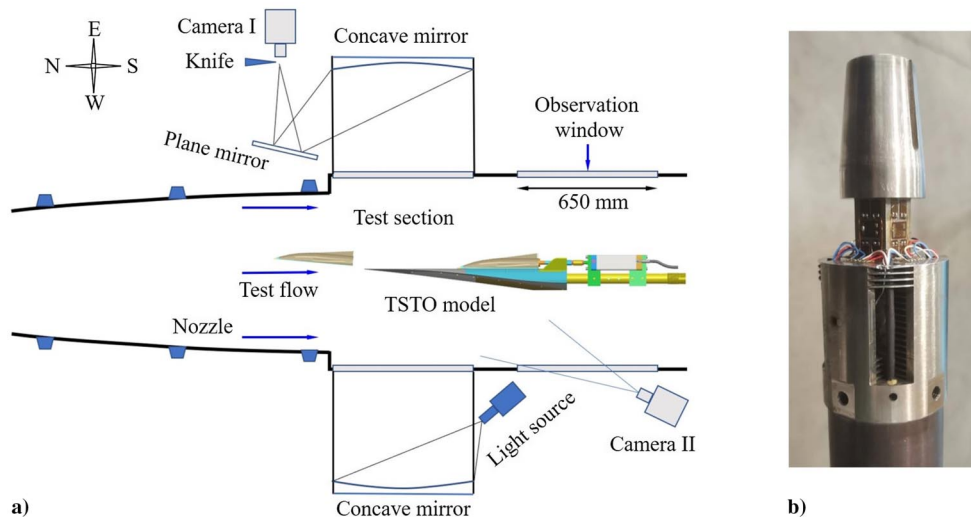

Fig. 1   Visualization system setup a) and six-component strain-gage balance b).
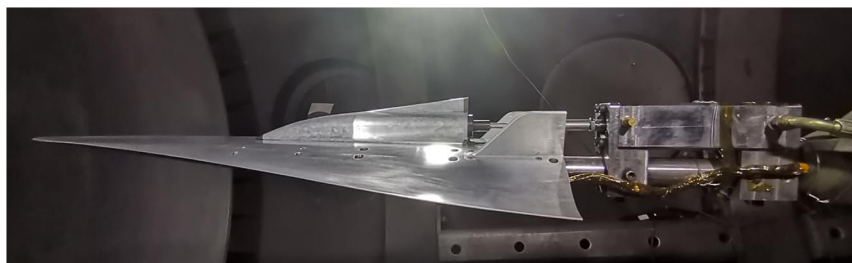

Fig. 2   A photograph of the TSTO model in the test section of the JF-12 shock tunnel.
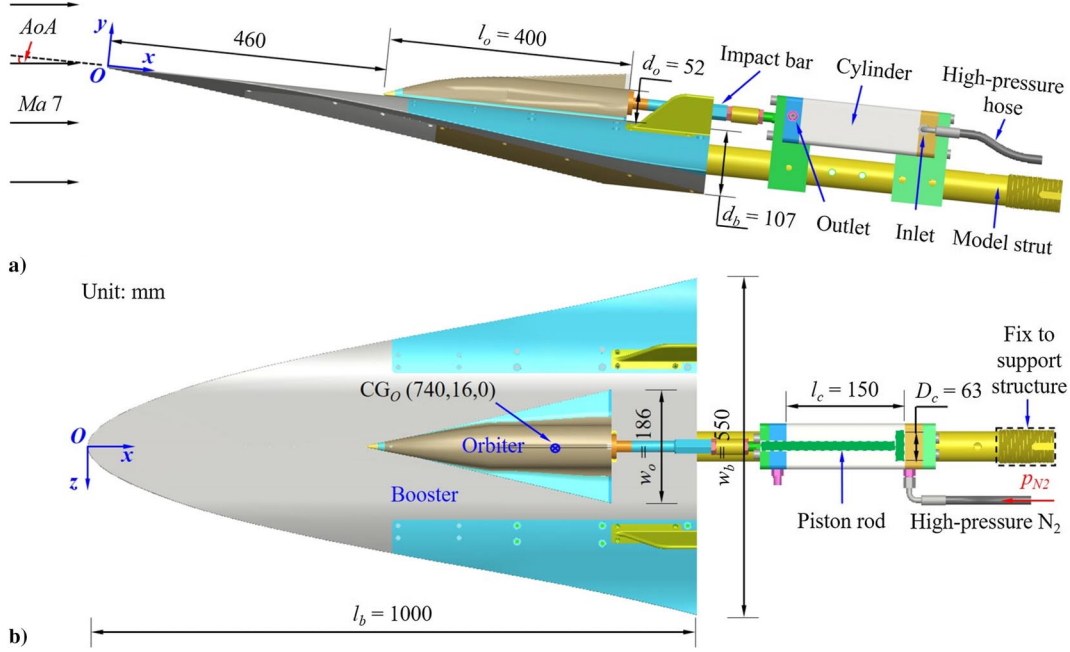
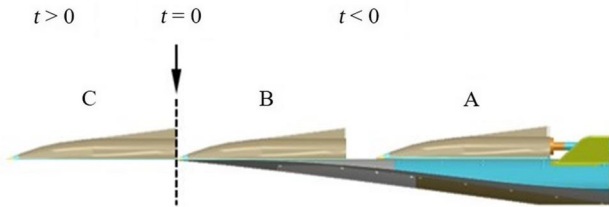Fig. 3 Geometry of the TSTO model and pneumatic actuator and supporting structure: a) side view; b) top view.

Fig. 4 Schematic of the separation movement of the orbiter.

The delay time of the PED (T_d) and separation duration of the orbiter (T_s) can be measured accurately by the visualization system in the ground atmosphere through several tests. Specifically, T_d includes the opening time of the solenoid valve, the ventilation time of nitrogen from the tee outlet to the inlet of the cylinder, and the actuation delay time of the cylinder. The solenoid valve opens quickly within 20 ms. Additionally, T_s is the sum of the time of separation phases I and II. Because the vacuum environment for the test is different from the ground environment with atmospheric pressure, the time of T_d and T_s in the vacuum environment is calibrated. If T_s is larger than T_e, the orbiter should move early to investigate and visualize separation phase II during T_e; otherwise, the orbiter moves after the test flowfield is constructed.

Fortunately, T_s is less than T_e due to the high-speed PED, and an ideal LSS test situation can be expected.

III. Results and Discussion

A. Aerodynamic Performance of TSTO

Figure 6 shows a schlieren photograph of the flowfields of the booster and TSTO static tests. Besides the weak orbiter shock on the nose, the leading-edge shock of the booster is composed of a strong oblique shock underneath and an upper weak oblique shock. The waverider configuration of the booster and such flowfields impart sound aerodynamic performance to the TSTO model. Table 2 presents the aerodynamics of static tests. Expressions of aerodynamic coefficients are shown in Eqs. (1–3), with "*" being substituted by "o" and "b" in the calculation of the orbiter and booster, respectively. The measured lift-to-drag can achieve 4 for the booster at AoA = 5 and 3.3 for TSTO at AoA = 8.1 deg, indicating the good aerodynamic performance of the TSTO model.

$$C_A = \frac{A}{q_\infty l_* w_*} \tag{1}$$

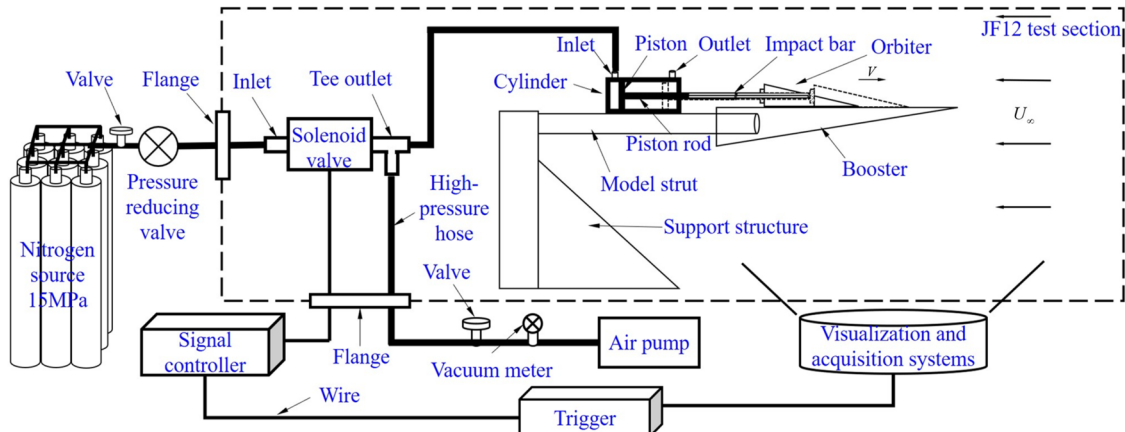$$C_N = \frac{N}{q_\infty l_* w_*} \tag{2}$$

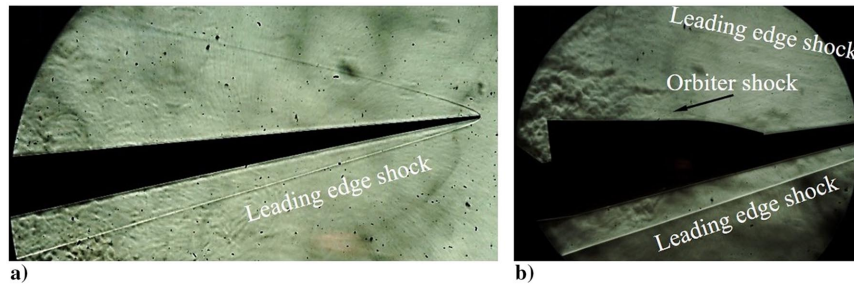Fig. 5 Schematic of the high-speed PED applied in the LSS dynamic test.

Fig. 6   Schlieren photographs of the booster a) and TSTO b) tests.

Table 2   Aerodynamic characteristics of static tests

Test	C_A	C_N	C_M	Lift-to-drag ratio
Booster	0.011	0.061	0.010	4.0
TSTO	0.015	0.098	0.014	3.3

$$C_M = \frac{M}{q_\infty l_*^2 w_*} \qquad (3)$$

B. Physical Flow During LSS

Figure 7 shows the pivotal changes in the flowfield during the LSS test at AoA = 8.3 deg. The flowfields of LSS are governed by the simple type I or VI oblique SSI [17] and the weak shock reflection in a small gap and weak oblique SBLI after the orbiter separates from the booster.

In phase I and most of phase II, neither gap nor SBLI occurs between stages under gravity and negative normal forces. At instant (a), the booster leading-edge shock and orbiter oblique shock occur with type VI SSI, which turns into a stronger convergent shock directly when the noses of the two stages coincide at instant (b). Moreover, the pressure along the upper surface of the booster is small, e.g., at $t = 7$ ms, as shown in Fig. 7a, due to no aerodynamic interference between stages but only the wake of the orbiter above the booster.

In addition, the type VI SSI occurs below the booster and affects the lower surface of the booster, as shown in Figs. 7c–7e. The transmitted oblique shock wave from type VI SSI "sweeps" over the lower surface of the booster with a tiny impinge angle, causing a pressure rise of about a maximum of 9% compared to the pressure on the "undisturbed" lower surface of the booster at the instant (h), as shown in Fig. 8b. In addition, as the impinge location moves upstream along the lower surface of the booster with the orbiter separates, the pressure on the forepart ($0.25 < x/l_b < 0.35$) increases, whereas that on the afterbody ($0.40 < x/l_b < 0.45$) decreases, as shown in Fig. 8b. However, the variation in pressure load within 9% is relatively small, resulting in little effect on the lower surface of the booster.
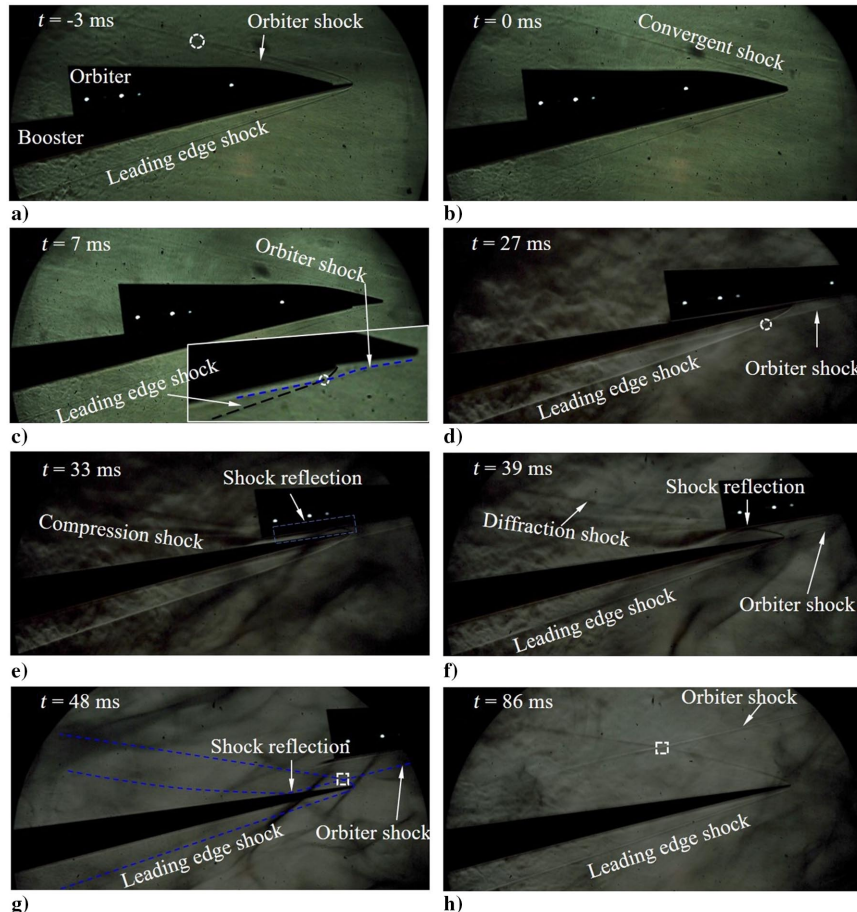

Fig. 7   Schlieren photographs and corresponding flow structures during LSS at AoA = 8.3 deg (circles denote type VI SSI, and squares denote type I SSI).
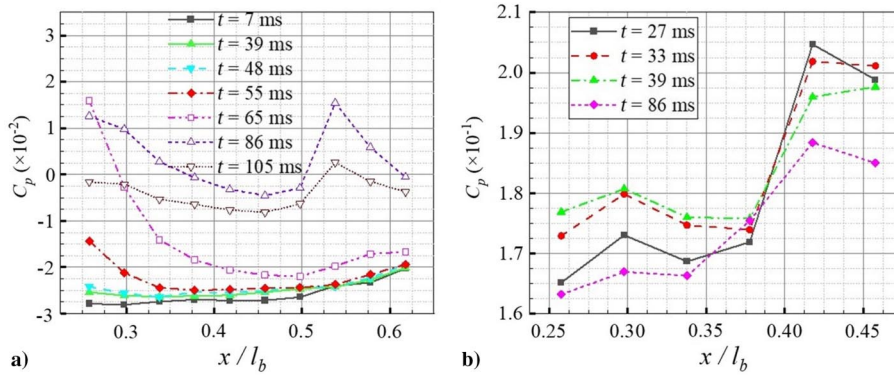
Fig. 8 Pressure coefficients on the booster during LSS test at AoA = 8.3 deg: a) along the upper surface; b) along the lower surface.

Moreover, the orbiter is lifted with a gap to the booster by the resultant normal force and the nose-up moment when the half fuselage of the orbiter separates from the booster, as shown in Figs. 7d–7f. A shock reflection occurs between the small gap, which can be observed at instants (e) and (f). Because the upstream flow encountering the booster is decelerated by the obiter oblique shock, the intensity of the leading-edge shock that impinges on the orbiter is decreased. Thus, the shock reflection is weak, and the reflected shock impinging on the upper surface of the booster does not induce a high pressure rise, as shown in Fig. 8a. Additionally, the compression shock is induced by the expansion of the flow out of the gap, as shown in Fig. 7e. The diffraction shock of the leading-edge shock of the booster is observed, as shown in Fig. 7f. As separation proceeds, the orbiter shock first interacts with the leading-edge shock in type I SSI and then impinges on the upper surface of the booster, resulting in SBLI. As the orbiter moves away from the booster, SBLI moves downstream along the upper surface of the booster, shown by the pressure response in Fig. 8a: the pressure coefficient along the upper surface of the booster increases as the shock reflection approaches and decreases as it moves away. Finally, the shock reflection disappears, and the only type I SSI remains in the flowfield and the isolated booster.

Figure 9 shows the schlieren photographs of flowfields and processes during the LSS test at AoA = 4.5 deg. The flow structures are similar to that shown in Fig. 7. The notable LSS character at AoA = 4.5 deg has no gap between stages during separation. Thus, no shock reflections or SBLI exists between stages or on the upper surface of the booster. The pressure loads on the booster are almost unchanged with no apparent pressure rise, as shown in Fig. 10. Moreover, as the orbiter separates, the pressure on the upper surface of the booster decreases slightly, which is affected by the wake flow of the orbiter. The pressure on the lower surface of the booster also decreases slightly because the type VI SSI vanishes. The aerodynamic interference in the LSS test at AoA = 4.5 deg is weaker than that at AoA = 8.3 deg.

C. Separation Motion of the Orbiter

The dimensionless separation traces' results of the LSS test at AoA = 8.3 and 4.5 deg are presented in Fig. 11 for reference. The set of the O-XYZ coordinate system is shown in Fig. 3. The trajectory quantitatively indicates that the orbiter is mainly separated in the axial direction, and the displacement in the normal direction is very small during LSS. For instance, the orbiter nearly separates along the upper surface of the booster with a constant axial velocity, and the drag in LSS does little effect on the deceleration. Moreover, the orbiter nearly separates along the booster with zero gap; i.e., the normal trajectory of Center of Gravity (CG) of the orbiter does not fluctuate, before $t = 0$ and $t = 10$ ms in LSS for AoA = 8.3 and 4.5 deg, respectively. When the orbiter is breaking through the leading-edge shock of the booster, the combined effect of normal forces and nose-up moment leads the orbiter to separate along the normal component direction. The effect occurs earlier and is more notable at higher AoA. Therefore, the orbiter does no obvious normal separation and very small normal velocity during the LSS test at AoA = 4.5 deg when compared to those at AoA = 8.3 deg. As for the test at AoA = 8.3 deg in Fig. 11a, the small variation in the pitching angle during LSS within 3 deg indicates stable separation. Moreover, a peak value of the pitching moment can be observed around $t = 0$ ms since the freestream and interference of booster leading-edge shock on the nose of the orbiter to cause a nose-up effect (which is also observed at AoA = 4.5 deg test shown in Fig. 11b); another peak value can be observed around $t = 35$ ms since the shock reflection occurs at the afterbody of the lower surface of the orbiter to cause a nose-down effect, as shown in Figs. 7e and 7f. The effect of the shock reflection prevents the further increase in the angular speed and corrects the pitching moment to a tiny value, which is conducive to the smooth separation of the orbiter. Its normal velocity increases steadily with the lift. Additionally, the pitching moment coefficient finally tends to a small nose-up moment. The test of AoA = 4.5 deg shows zero gaps during the whole separation, smaller axial and normal forces, but a notable nose-down moment compared with
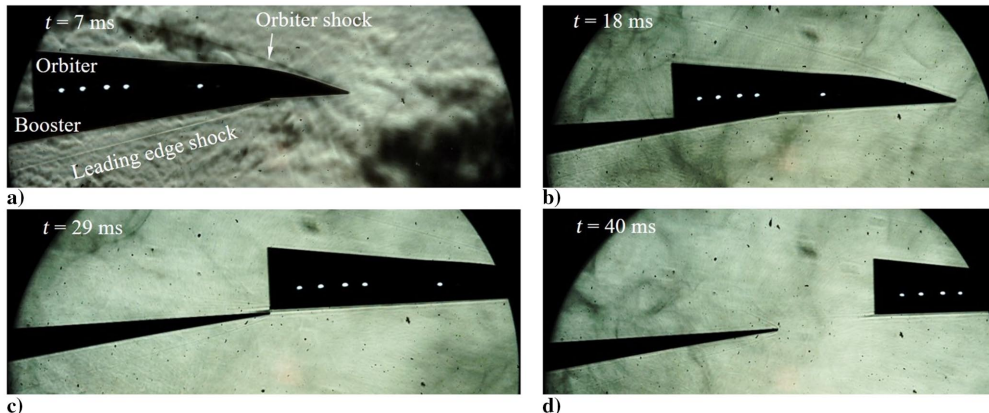

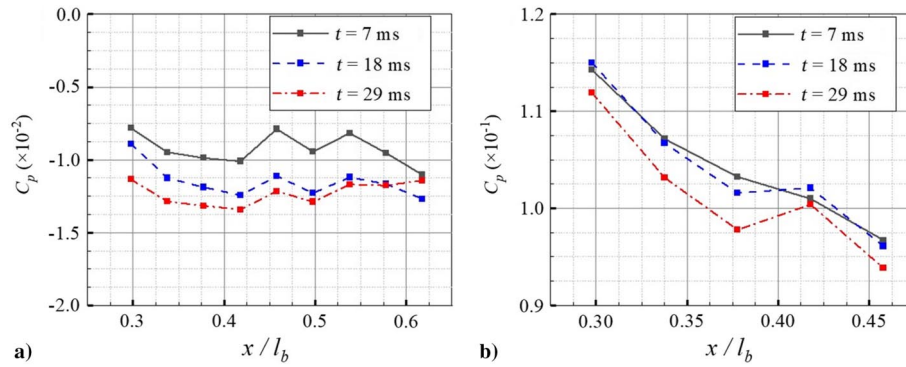**Fig. 9 Schlieren photographs of LSS at AoA = 4.5 deg.**

Fig. 10   Pressure coefficients on the booster during the LSS test at AoA = 4.5 deg: a) along the upper surface; b) along the lower surface.
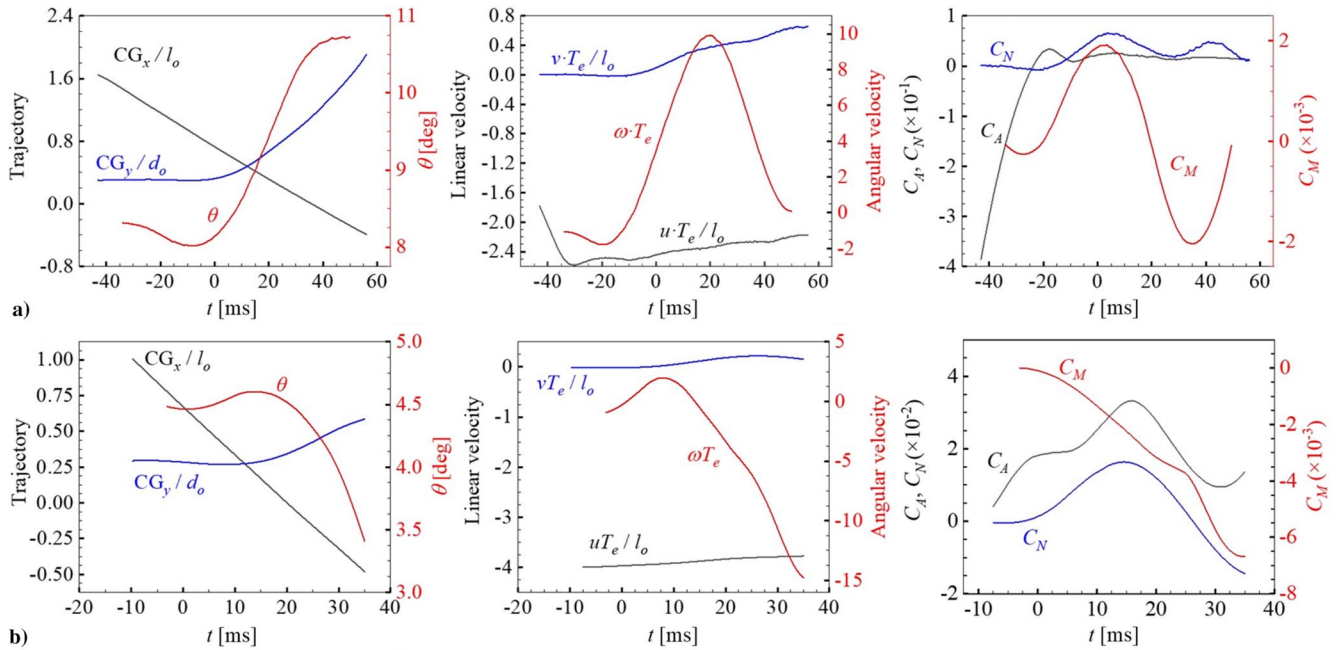

Fig. 11   Separation trace results of the LSS test at a) AoA = 8.3 deg and b) AoA = 4.5 deg.

those in the test of AoA = 8.3 deg, as shown in Fig. 11b. When the orbiter separates from the booster, the tiny negative normal force (nearly zero) becomes positive due to the interference of the leading-edge shock of the booster with the lower surface of the orbiter, as shown in Figs. 9a–9c. However, this tendency reverses after separation. The negative normal force and nose-down moment increase as the pitching angle decreases, and vice versa. Figure 12 presents the photographs of high-speed camera II for separation at AoA = 8.3 deg for reference, with the orbiter stably separating from the booster.

Although the static stage separation test is not conducted in this study, the differences between the static and dynamic stage separation of TSTO should be noted and claimed here for the significance of dynamic stage separation of TSTO in JF-12 shock tunnel. Firstly, the

static separation test cannot duplicate the exact positions of the dynamic separation trace because the separation positions and attitudes of the orbiter cannot be acquired in advance. Secondly, the static separation test cannot duplicate the unsteady effects dominated by the coupled effects of complex aerodynamic interference and multibody motion in hypersonic flow. Thirdly, the static separation test will introduce the additional interference from the model support structure to the flowfield. Hence, the dynamic stage separation test reveals the essential mechanism of the unsteady flow and accuracy compared to the static test. Moreover, the dynamic stage separation test for TSTO in JF-12 shock tunnel duplicates the reliable hypersonic flight condition and high-temperature gas effects during Mach 7 stage separation.
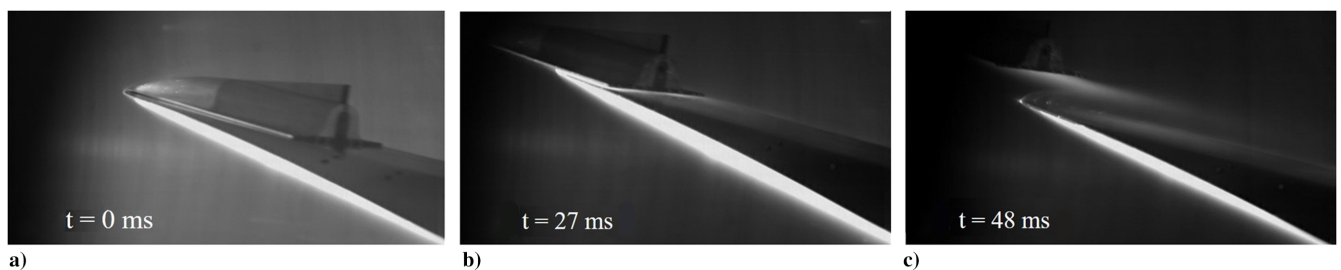

Fig. 12   High-speed camera II photographs of the LSS test at AoA = 8.3 deg.

IV. Conclusions

This study is the first to report the tests of a parallel-staged TSTO model with dynamic LSS stage separation at different AoA values in the JF-12 hypersonic flight duplicated shock tunnel. The high-speed PED is developed for the dynamic test technique in a shock tunnel. Static tests show the good aerodynamic performance of the TSTO model. Dynamic tests show that the small stage gap of LSS leads to weak type I and VI SSI, with short-time weak shock reflection and weak oblique SBLI in the flowfield at high AoA values. Furthermore, no shock reflection or weak oblique SBLI is observed in LSS at small AoA values, so the aerodynamic interference of LSS is weak. In addition, although the orbiter exhibits a smooth separation maneuver in both LSS tests, it tends to fly in a nose-up attitude at AoA = 8.3 deg and a nose-down flight attitude at AoA = 4.5 deg. Hence, the most appropriate AoA condition for the LSS of the TSTO model may be expected in the middle of 4.5 and 8.3 deg. No stage recontact is observed during LSS, and the safety and feasibility of LSS for the parallel-staged TSTO model are demonstrated experimentally, which is important for the success of the future TSTO system. In future work, LSS tests will be conducted under more AoA conditions to further verify the most appropriate condition for the LSS of TSTO. The effects of AoA on LSS characteristics and detailed flowfields should be investigated in combination with numerical simulations.

Acknowledgments

References

[1] Fedorov, A. V., Soudakov, V. G., and Malmuth, N. D., "Theoretical Modeling of Two-Body Interaction in Supersonic Flow," *AIAA Journal*, Vol. 48, No. 2, 2010, pp. 258–266.
https://doi.org/10.2514/1.40592

[2] Wang, Y., Ozawa, H., Koyama, H., and Nakamura, Y., "Abort Separation of Launch Escape System Using Aerodynamic Interference," *AIAA Journal*, Vol. 51, No. 1, 2012, pp. 270–275.
https://doi.org/10.2514/1.J051627

[3] Xue, X.-P., Nishiyama, Y., Nakamura, Y., Mori, K., and Wen, C.-Y., "Parametric Study on Aerodynamic Interaction of Supersonic Parachute System," *AIAA Journal*, Vol. 53, No. 9, 2015, pp. 2796–2801.
https://doi.org/10.2514/1.J053824

[4] Moelyadi, M. A., Breitsamter, C., and Laschka, B., "Stage-Separation Aerodynamics of Two-Stage Space Transport Systems Part 2: Unsteady Simulation," *Journal of Spacecraft and Rockets*, Vol. 45, No. 6, 2008, pp. 1240–1250.
https://doi.org/10.2514/1.35059

[5] Schroder, W., and Hartmann, G., "Analysis of Inviscid and Viscous Hypersonic Flows Past a Two-Stage Spacecraft," *Journal of Spacecraft and Rockets*, Vol. 30, No. 1, 1993, pp. 8–13.
https://doi.org/10.2514/3.25465

[6] Cheng, J., Chen, R., Qiu, R., Sun, W., and You, Y., "Aerothermodynamic Study of Two-Stage-to-Orbit System Composed of Wide-Speed-Range Vehicle and Rocket," *Acta Astronautica*, Vol. 183, June 2021, pp. 330–345.
https://doi.org/10.1016/j.actaastro.2020.11.034

[7] Liu, Y., Qian, Z., Lu, W., and He, S., "Numerical Investigation on the Safe Stage-Separation Mode for a TSTO Vehicle," *Aerospace Science and Technology*, Vol. 107, 2020, Paper 106349.
https://doi.org/10.1016/j.ast.2020.106349

[8] Bordelon, W., Frost, A., and Reed, D., "Stage Separation Wind Tunnel Tests of a Generic TSTO Launch Vehicle," *21st AIAA Applied Aerodynamics Conference*, AIAA Paper 2003-4227, 2003.
https://doi.org/10.2514/6.2003-4227

[9] Ozawa, H., Hanai, K., Kitamura, K., Mori, K., and Nakamura, Y., "Experimental Investigation of Shear-Layer/Body Interactions in TSTO at Hypersonic Speeds," *46th AIAA Aerospace Sciences Meeting and Exhibit*, AIAA Paper 2008-723, 2008.
https://doi.org/10.2514/6.2008-723

[10] Liever, P., and Habchi, S., "Separation Analysis of Launch Vehicle Crew Escape Systems," *22nd Applied Aerodynamics Conference and Exhibit*, AIAA Paper 2004-4726, 2004.
https://doi.org/10.2514/6.2004-4726

[11] Wang, Y., Wang, Y. P., Xue, X. P., and Jiang, Z. L., "Numerical Investigation on Safe Stage Separation Problem of a TSTO Model at Mach 7," *Chinese Journal of Theoretical and Applied Mechanics*, Vol. 54, No. 2, 2022, pp. 526–542.
https://doi.org/10.6052/0459-1879-21-423

[12] Breitsamter, C., Laschka, B., Zaehringer, C., and Sachs, G., "Wind Tunnel Tests for Separation Dynamics Modeling of a Two-Stage Hypersonic Vehicle," *10th AIAA/NAL-NASDA-ISAS International Space Planes and Hypersonic Systems and Technologies Conference*, AIAA Paper 2001-1811, 2001.
https://doi.org/10.2514/6.2001-1811

[13] Black, R., and Picklesimer, J., "Captive Trajectory Technique Improvements of Store Separation Studies in a Wind Tunnel," *6th Aerodynamics Testing Conference*, AIAA Paper 1971-282, 1971.
https://doi.org/10.2514/6.1971-282

[14] Lin, J., "China's First Hypersonic Wind Tunnel Dual CTS Test Capability Formed in CARDC," *Journal of Experiments in Fluid Mechanics*, Vol. 35, No. 1, 2021, p. 126.

[15] Jiang, Z., "Experiments and Development of Long-Test-Duration Hypervelocity Detonation-Driven Shock Tunnel (LHDst)," *52nd Aerospace Sciences Meeting*, AIAA Paper 2014-1012, 2014.
https://doi.org/10.2514/6.2014-1012

[16] Wang, Y., Hu, Z., Liu, Y., and Jiang, Z., "Starting Process in a Large-Scale Shock Tunnel," *AIAA Journal*, Vol. 54, No. 4, 2016, pp. 1240–1249.
https://doi.org/10.2514/1.J054145

[17] Edney, B. E., "Effects of Shock Impingement on the Heat Transfer Around Blunt Bodies," *AIAA Journal*, Vol. 6, No. 1, 1968, pp. 15–21.
https://doi.org/10.2514/3.4435

C. Lee
Associate Editor